International Journal of Remote Sensing
Vol. 27, No. 14, 20 July 2006, 3049–3055

Taylor & Francis
Taylor & Francis Group

Fire detection in imaging spectrometer data using atmospheric carbon dioxide absorption

P. E. DENNISON
Center for Natural and Technological Hazards, Department of Geography, 260 S. Central Campus Dr. Rm. 270, University of Utah, Salt Lake City, Utah 84112, USA.
e-mail: dennison@geog.utah.edu

(*Received 13 January 2006; in final form 28 February 2006*)

Fire detection in shortwave infrared (SWIR) imaging spectrometer data should be possible using the proportion of reflected and emitted radiance absorbed by atmospheric carbon dioxide. A continuum interpolated band ratio (CIBR) was used to measure the relative depth of the 2000 nm carbon dioxide absorption band. Low CIBR values indicated dominantly reflected radiance, while high CIBR values indicated dominantly emitted radiance and the presence of active fire. CIBR values were calculated for Airborne Visible/InfraRed Imaging Spectrometer (AVIRIS) and Hyperion hyperspectral data over fires in California and Arizona. The proposed algorithm has potential uses for fire detection and improving the efficiency of fire temperature retrieval from imaging spectrometer data.

1. Introduction

The impacts of wildfires span scales from local (e.g. habitat destruction) to global (e.g. the global carbon cycle). Detection of wildfires using remote sensing data allows estimation of the location, frequency, and potential effects of wildfires over large areas. Fire detection algorithms have been developed for a variety of mid-infrared and thermal infrared multispectral sensors (e.g. Kaufman *et al.* 1990, Prins and Menzel 1992, Kaufman *et al.* 1998, Giglio *et al.* 2003, Ichoku *et al.* 2003). In comparison, there has been relatively little exploration of fire detection algorithms for hyperspectral data. For instance, Green (1996) used the spectral shape of fire-emitted radiance to model fire temperature from AVIRIS data. Vodacek *et al.* (2002) proposed a hyperspectral fire detection algorithm based on potassium emission lines at 767 nm and 770 nm, corresponding to the ratio of an AVIRIS band containing the potassium emission to an adjacent band. However, dense smoke has the potential to obscure near infrared potassium emission (Vodacek *et al.* 2002). Dennison *et al.* (2006) further developed the Green (1996) algorithm and demonstrated that smoke contamination in the visible and near infrared restricted the useful wavelength range for retrieving fire temperature. Dennison *et al.* (2006) found only minor smoke impacts in the shortwave infrared. The goal of this study is to propose a hyperspectral fire detection algorithm that minimizes smoke contamination issues by comparing emitted and reflected radiance within a shortwave infrared carbon dioxide absorption band.

2. Methods

The SWIR radiance measured by a sensor imaging a fire in daylight is a combination of reflected solar radiance, emitted radiance, and path radiance. The

International Journal of Remote Sensing
ISSN 0143-1161 print/ISSN 1366-5901 online
http://www.tandf.co.uk/journals
DOI: 10.1080/01431160600660871

wavelength-specific, at-sensor radiance ($L_{\lambda t}$) is:

$$L_{\lambda t} = L_{\lambda r} + L_{\lambda Pr} + L_{\lambda e} + L_{\lambda Pe} \quad (1)$$

where $L_{\lambda r}$ is the reflected solar radiance, $L_{\lambda Pr}$ is the reflected solar path radiance, $L_{\lambda e}$ is the emitted radiance, and $L_{\lambda Pe}$ is the emitted path radiance. If the path radiance terms are assumed negligible in the SWIR, equation (1) becomes:

$$L_{\lambda t} = L_{\lambda r} + L_{\lambda e} \quad (2)$$

Assuming that the incoming solar irradiance is reflected off a Lambertian surface, the reflected solar path radiance is corrected for plane-parallel atmospheric absorption is:

$$L_{\lambda r} = \frac{E_{\lambda 0}\rho_{\lambda} e^{-\alpha_{\lambda} d \sec\theta} e^{-\alpha_{\lambda} d \sec\phi} \cos\theta}{\pi} \quad (3)$$

where $E_{\lambda 0}$ is the exoatmospheric solar irradiance, θ is the solar zenith angle, ρ_{λ} is the reflectance of the surface, α_{λ} is the atmospheric absorption coefficient, $d \sec\theta$ is the incoming path length corrected for solar zenith angle and $d \sec\phi$ is the outgoing path length corrected for sensor view zenith angle. Incoming solar irradiance is reduced by atmospheric absorption along the upwelling and downwelling path. Emitted radiance, however, is subject to absorption only along the upwelling path:

$$L_{\lambda e} = L_{\lambda 0} e^{-\alpha_{\lambda} d \sec\phi} \quad (4)$$

where $L_{\lambda 0}$ is the initial upwelling radiance.

Spectral differences in atmospheric absorption should allow separation of dominantly emitted radiance from dominantly reflected radiance. In a strong atmospheric absorption band, emitted radiance should show decreased absorption relative to reflected radiance due to its shorter path length. Adjacent regions of the spectrum possessing weak atmospheric absorption can be used as reference bands. A continuum interpolated band ratio (CIBR) can be used to determine the relative contributions of reflected and emitted radiance:

$$CIBR = \frac{L_{\lambda_1}}{w_2 L_{\lambda_2} + w_3 L_{\lambda_3}} \quad (5)$$

where λ_1 is a wavelength within the strong absorption band and λ_2 and λ_3 are wavelengths outside the strong absorption band (Gao and Goetz 1990). Weighting factors w_2 and w_3 are proportional to the wavelength differences between λ_1 and λ_2, and between λ_1 and λ_3. The lowest CIBR values will occur for purely reflected radiance and the highest CIBR values will occur for purely emitted radiance. Mixtures of reflected and emitted radiance will possess a CIBR between the two extremes for purely reflected and purely emitted radiance.

This CIBR can be used to detect emitted radiance from fires, as long as several additional variables from equations (3) and (4) are taken into account. First, changes in path length due to elevation, solar zenith, or sensor view zenith will result in changes in CIBR values. Differences in surface reflectance between CIBR bands and changes in carbon dioxide concentrations and reflectance over space will also affect the CIBR. In most cases, changes in reflected radiance caused by variable path length, carbon dioxide concentration and surface reflectance within an image will be

much smaller than changes caused by emitted radiance, but variability in reflected radiance may increase the CIBR threshold used to detect active fires.

A carbon dioxide absorption band at approximately 2000 nm was used to test whether the CIBR could be used to detect fires in imaging spectrometer data. Vibrational absorption causes a trio of absorption features in the SWIR (figure 1). The shortest wavelength absorption peak is normally obscured by strong atmospheric water vapour absorption from 1780 nm to 1970 nm, but the remaining two absorption peaks are distinct in imaging spectrometer data. HITRAN (Rothman *et al.* 2003) was used to calculate the absorption spectrum of carbon dioxide.

The carbon dioxide CIBR was calculated for a high-resolution AVIRIS radiance image acquired over the 2003 Simi Fire in Southern California and a Hyperion radiance image acquired over the 2003 Aspen Fire in Southern Arizona. The AVIRIS image was acquired with a 5-m ground instantaneous field of view (GIFOV) and a solar zenith of 51.6°, over an area with elevation ranging from approximately 650 to 1100 m (for more detail, see Dennison *et al.* 2006). The Hyperion image was acquired with a 30-m GIFOV and a solar zenith of 10.3°, over an area with elevation ranging from approximately 650 to 2800 m. The HITRAN absorption spectrum was convolved to 2003 AVIRIS and Hyperion bands using the band centres and full-width half maxima for each sensor and a Gaussian function (figure 1). Peak absorption was determined to occur within the 2000 nm AVIRIS band (band 173) and the 2002 nm Hyperion band (band 185). These bands were used as the CIBR numerator. Reference bands at 1980 nm and 2041 nm for AVIRIS (bands 171 and 177) and 1982 nm and 2042 nm for Hyperion (bands 183 and 189) were determined to have minimal carbon dioxide absorption, and were used in the

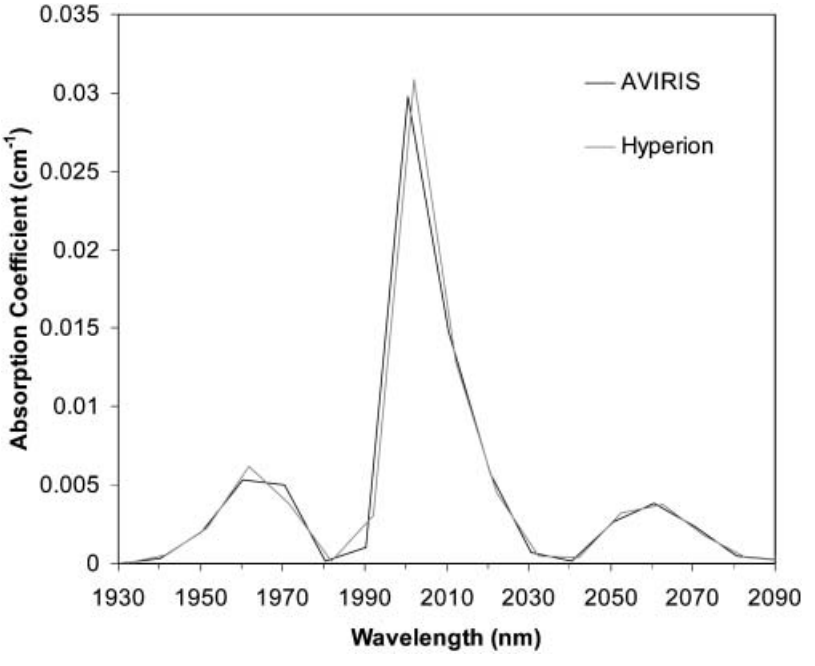

Figure 1. The HITRAN carbon dioxide absorption spectrum convolved to AVIRIS and Hyperion bands.

CIBR denominator. Weighting factors of 0.666 for the shorter wavelength reference band and 0.334 for the longer wavelength reference band were used to calculate both the AVIRIS and Hyperion CIBRs.

3. Results and discussion

The CIBR image calculated from the AVIRIS image of the Simi Fire shows high contrast between actively burning areas with high CIBR values and non-burning areas with low CIBR values (figure 2). Sensor saturation due to high SWIR emission is evident along the fire front, where the hottest fires occurred (Dennison *et al.* 2006). A black ring surrounding the hottest fires (figure 2, to the right of 'A')

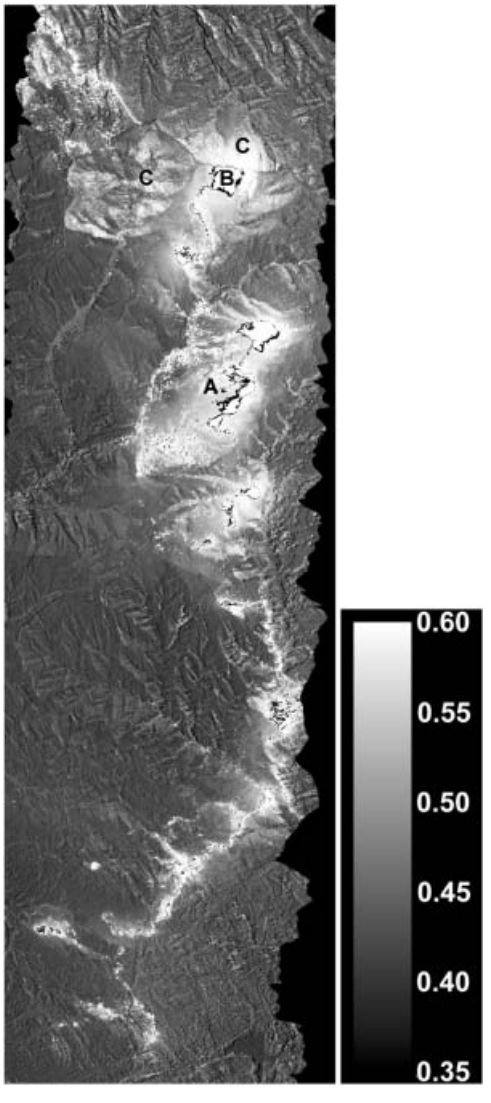

Figure 2. The carbon dioxide CIBR calculated for a subset of the 2003 Simi Fire AVIRIS image. This image was acquired on 27 October 2003 at approximate latitude and longitude 34.4° N, 118.7° W.

denotes areas where one or both of the reference bands saturated, but the carbon dioxide absorption band did not saturate, producing a very low CIBR. Inside this black ring, the white areas indicate where all three bands used to calculate the CIBR saturated (figure 2, marked 'B'), producing a very high CIBR. Outside the saturated areas, the CIBR demonstrates evidence of high radiant emission fires burning along the fire front and lower radiant emission fires burning behind (to the left of) the fire front. Figure 2 'C' marks areas with lower CIBR values that correspond to lower temperature burning or smoldering mapped by Dennison *et al*. (2006). Individual riparian tree canopies burning behind the fire front are visible to the left of 'B' in figure 2. While the CIBR of the non-burning areas is overall much lower than the CIBR of the actively burning areas, there is considerable variation in the CIBR of non-burning areas. This variation is predominantly caused by sensor noise within pixels possessing low reflected radiance, either due to low reflectance surfaces such as dark ash or dense vegetation, or due to topographic shadows.

The CIBR values calculated from Hyperion data are lower than those calculated from AVIRIS data because Hyperion is a spaceborne sensor, resulting in a much longer path length. Hyperion has a lower signal-to-noise ratio than AVIRIS (Roberts *et al*. 2003), and the effects of sensor noise on the CIBR are very apparent in figure 3. Actively burning areas still stand out with the highest CIBR values, but non-burning areas exhibit higher variation in the Hyperion CIBR image. CIBR values are lowest in the upper right corner of the image, where elevations are lowest. Vertical striping and artificially high CIBR values on the right edge of the image are caused by variation in the sensor response functions of the detectors within the Hyperion linear array.

Fire detection using a carbon dioxide CIBR would rely on determining an appropriate threshold above which the CIBR would indicate an active fire. This threshold would vary based on elevation, solar zenith, and albedo. The shortwave infrared wavelength region used by the carbon dioxide CIBR avoids contamination

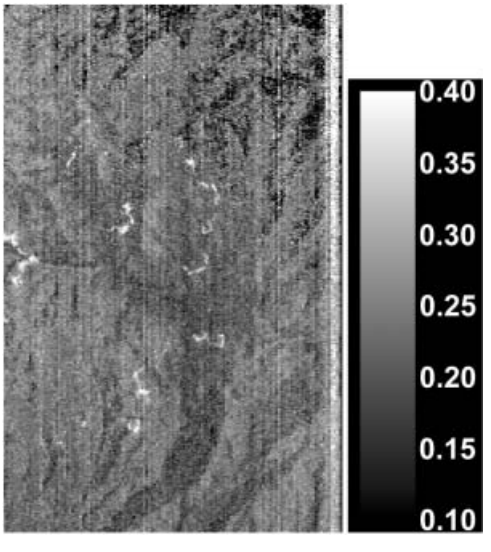

Figure 3. The carbon dioxide CIBR calculated for a subset of the 2003 Aspen Fire Hyperion image. This image was acquired on 3 July 2003, at the approximate latitude and longitude 32.3° N, 110.8° W.

by smoke and increases the available emitted radiance, at the expense of the available reflected radiance, which decreases with wavelength. Sensor noise (for low measured radiance) and sensor saturation (for high measured radiance) may limit the ability of a threshold approach to map active fires.

Using a radiative transfer model, it may be possible to develop a simple model of the CIBR for a given set of environmental conditions. Deviations from the predicted values would indicate the presence of fire. With further development, the CIBR could be used in combination with hyperspectral temperature retrieval, as demonstrated by Green (1996) and Dennison *et al*. (2006). A CIBR threshold would be used to limit temperature modelling to only those pixels that contain a sufficiently high CIBR. Temperature and fire fractional area estimated by the more complex model would allow description of combustion characteristics at a greatly reduced computational cost. Finally, it is worth noting that increased carbon dioxide absorption was not observed in the smoke plumes of the Simi Fire, indicating that the increased carbon dioxide concentrations caused by combustion may be too low to be detectable using AVIRIS data. Both increased carbon dioxide concentrations and radiant emission within carbon dioxide absorption bands should be detectable by more sensitive future imaging spectrometers designed to measure atmospheric constituents, such as the proposed Orbiting Carbon Observatory mission.

Acknowledgements

The author would like to thank the Jet Propulsion Laboratory for providing AVIRIS data and the United States Geological Survey for providing Hyperion data. The author also thanks the reviewers for their helpful comments.

References

Dennison, P.E., Charoensiri, K., Roberts, D.A., Peterson, S.H. and Green, R.O., 2006, Wildfire temperature and land cover modeling using hyperspectral data. *Remote Sensing of Environment*, **100**, pp. 212–222.

Gao, B.C. and Goetz, A.F.H., 1990, Column atmospheric water vapor and vegetation liquid water retrievals from airborne imaging spectrometer data. *Journal of Geophysical Research*, **95**, pp. 3549–3564.

Giglio, L., Descloitres, J., Justice, C.O. and Kaufman, Y.J., 2003, An enhanced contextual fire detection algorithm for MODIS. *Remote Sensing of Environment*, **87**, pp. 273–282.

Green, R.O., 1996, Estimation of biomass fire temperature and areal extent from calibrated AVIRIS spectra. Summaries of the Sixth Annual JPL Airborne Earth Science Workshop, Pasadena: Jet Propulsion Laboratory, JPL Publication 96-4 Volume 1, pp. 105–113.

Ichoku, C., Kaufman, Y.J., Giglio, L., Li, Z., Fraser, R.H., Jin, J.Z. and Park, W.M., 2003, Comparative analysis of daytime fire detection algorithms using AVHRR data for the 1995 fire season in Canada: Perspective for MODIS. *International Journal of Remote Sensing*, **24**, pp. 1669–1690.

Kaufman, Y.J., Tucker, C.J. and Fung, I., 1990, Remote sensing of biomass burning in the tropics. *Journal of Geophysical Research*, **95**, pp. 9927–9939.

Kaufman, Y.J., Justice, C.O., Flynn, L.P., Kendall, J.D., Prins, E.M., Ward, D.E., Menzel, W.P. and Setzer, A.W., 1998, Potential global fire monitoring from EOS-MODIS. *Journal of Geophysical Research*, **103**, pp. 32215–32238.

Prins, E.M. and Menzel, W.P., 1992, Geostationary satellite detection of biomass burning in South America. *International Journal of Remote Sensing*, **13**, pp. 2783–2799.

ROBERTS, D.A., DENNISON, P.E., GARDNER, M., HETZEL, Y.L., USTIN, S.L. and LEE, C., 2003, Evaluation of the potential of Hyperion for fire danger assessment by comparison to the Airborne Visible Infrared Imaging Spectrometer. *IEEE Transactions on Geoscience and Remote Sensing*, **41**, pp. 1297–1310.

ROTHMAN, L.S., BARBE, A., CHRIS BENNER, D., BROWN, L.R., CAMY-PEYRET, C., CARLEER, M.R., CHANCE, K., CLERBAUX, C., DANA, V., DEVI, V.M., FAYT, A., FLAUD, J.-M., GAMACHE, R.R., GOLDMAN, A., JACQUEMART, D., JUCKS, K.W., LAFFERTY, W.J., MANDIN, J.-Y., MASSIE, S.T., NEMTCHINOV, V., NEWNHAM, D.A., PERRIN, A., RINSLAND, C.P., SCHROEDER, J., SMITH, K.M., SMITH, M.A.H., TANG, K., TOTH, R.A., VANDER AUWERA, J., VARANASI, P. and YOSHINO, K., 2003, The HITRAN molecular spectroscopic database: edition of 2000 including updates through 2001. *Journal of Quantitative Spectroscopy and Radiative Transfer*, **82**, pp. 5–44.

VODACEK, A., KREMENS, R.L., FORDHAM, A.J., VANGORDEN, S.C., LUISI, D., SCHOTT, J.R. and LATHAM, D.J., 2002, Remote optical detection of biomass burning using a potassium emission signature. *International Journal of Remote Sensing*, **13**, pp. 2721–2726.